BRNO UNIVERSITY OF TECHNOLOGY
VYSOKÉ UČENÍ TECHNICKÉ V BRNĚ

FACULTY OF ELECTRICAL ENGINEERING AND COMMUNICATION
FAKULTA ELEKTROTECHNIKY
A KOMUNIKAČNÍCH TECHNOLOGIÍ

DEPARTMENT OF PHYSICS
ÚSTAV FYZIKY

NOISE, TRANSPORT AND STRUCTURAL PROPERTIES OF HIGH ENERGY RADIATION DETECTORS BASED ON CDTE
TRANSPORTNÍ, ŠUMOVÉ A STRUKTURÁLNÍ VLASTNOSTI DETEKTORŮ VYSOKOENERGETICKÉHO ZÁŘENÍ NA BÁZI CDTE

DOCTORAL THESIS - SHORT VERSION
DIZERTAČNÍ PRÁCE - TEZE

AUTHOR
AUTOR PRÁCE
Ing. Ondřej Šik

SUPERVISOR
ŠKOLITEL
prof. Ing. Lubomír Grmela, CSc.

BRNO 2016

Keywords: CdTe, CdZnTe, thermal degradation, noise, metal-semiconductor junction, elemental concentration depth profile, surface modification, heterostructure, polarization, electric field distribution, SIMS, XPS, Auger, XRD, ion bombardment.

Klíčová slova CdTe, CdZnTe, teplotní degradace, šum, přechod polovodič-kov, hloubkový profil prvkového složení, modifikace povrchu, heterostruktura, polarizace, rozložení elektrického pole, SIMS, XPS, Auger, XRD, bombardování ionty.

Disertační práce je k dispozici na Vědeckém oddělení děkanátu Fakulty elektrotechniky a komunikačních technologií VUT v Brně, Technická 3058/10, Brno, 616 00.

ŠIK, O. *Transportní, šumové a strukturální vlastnosti detektorů vysokoenergetického záření na bázi CdTe.*. Brno: Vysoké učení technické v Brně, Fakulta elektrotechniky a komunikačních technologií, 2016. 28 s. Zkrácená verze disertační práce. Vedoucí disertační práce prof. Ing. Lubomír Grmela, CSc.

CONTENT

1 INTRODUCTION 1

2 STATE-OF-ART 1

2.1 Crystal growth 2
2.2 Contacts 3
2.3 Surface 3
2.4 Noise 4

3 EXPERIMENTAL RESULTS 6

3.1 Localization of the leakag current and noise sources in CdZnTe detector system 6
3.2 Electric fieald distribution and noise evolution during the polarization 10
3.2.1 Electric field distribution during polarization 10
3.2.2 Evolution of noise during polarization 11
3.3 Analysis of the contact symmetry and its impact on the low frequency noise. 11
3.4 Investigation of thermal stress effect on CdTe detectors 13
3.4.1 Analysis of the effect of thermal stressing on charge transport properties 13
3.4.2 Structural investigation: XPS depth profiling of the M-S structure 15
3.5 Investigation of the effect of the argon ion beam on CdZnTe single crystals surface structural properties 18
3.5.1 SEM study of irradiated surface 18
3.5.2 AFM and XPS study of irradiated surface 20

4 CONCLUSION 22

ABSTRACT 24

ABSTRAKT 24

REFERENCES 25

LIST OF SELECTED PUBLICATIONS – PUBLISHED IN JOURNALS WITH IMPACT FACTOR 26

CURRICULUM VITAE 28

1 INTRODUCTION

Because of demands from space research, healthcare and nuclear safety industry, gamma and X-ray imaging and detection is rapidly growing topic of research. Many materials are studied to develop detectors with high stopping power, high spectral resolution and capability of imaging. Because of its high atomic number and high density, scintillators are frequent instrumentation for X-ray sensing. Nevertheless, their biggest disadvantage is the low spectral resolution. Semiconductors offer the benefit of direct conversion, have presumptions to give excellent spectral resolution and well developed lithographic technologies predestine semiconductors as a successful candidate for X-ray imaging.

Most common semiconducting materials like Si, Ge can provide good energy resolution, but Si offers low stopping power and Ge has small band gap that requires cryogenic conditions for operation. Improved manufacturing technology, gave the possibility for development of a new semiconductor material with high atom number, relatively high density and wide bandgap – CdTe /and its alloy CdZnTe. These materials are suitable to detect high energy photons in range from 10 keV to 500 keV. Their 1.46 -1.6 eV band gap gives the possibility of high resistivity (10^{10}-10^{11} Ωcm) crystals production that is high enough for room temperature operation. Even though research of CdTe / CdZnTe started in 1970s, the most significant progress in crystal quality and better availability of CdTe / CdZnTe on the market happened in recent years.

In spite of recent progress, the quality of CdTe CdZnTe detectors is still far from perfect. Compared to Si, CdTe / CdZnTe crystals exhibit higher concentration of defects. It is difficult to obtain large volume (>1 cm^3) crystals suitable for > 500 keV photons detection. Large work function of CdTe / CdZnTe and not well defined properties of the surface brings difficulties in proper crystal metallization. From these imperfections, three basic issues arise for CdTe / CdZnTe detectors: i) lower resistance of the detector than the theoretical one, ii) higher additive noise and iii) instability of spectral sensitivity and electrical parameters in time. Such difficulties limit the performance, especially for operation under high fluxes of radiation.

Above mentioned facts led me to investigate the properties of CdTe/CdZnTe detectors under various states of their defectiveness. Investigation of detector grade crystals, crystals with lower resistivity and enhanced polarization, detectors with asymmetry of electrical characteristics and thermally degenerated crystals were subject of my work in terms of analysis of their current stability, additional noise, electric field distribution and structural properties.

2 STATE-OF-ART

Effective atomic number 48.5, density of 5.6 g/cm^3, reasonable electron mobility ~1000 cm/Vs and the mobility- lifetime product ~10^{-3} cm^2/V mm are good preconditions for a spectroscopic X-ray detector made from CdTe / CdZnTe. CdTe

based radiation detector is a system, whose parameters are affected by three key parts: i) Detector active volume (Crystal), ii) Points of biasing and signal extraction (metal contacts) and iii) Detector surface. All of these have crucial effect on the properties of the detector and none of them can be neglected in the manufacturing process and analysis.

2.1 CRYSTAL GROWTH

Development of high-resistivity single crystals (ρ = 10^{10} Ωcm) is done by optimization of the crystal growth technologies based on traditional melt-growth or vapour-growth techniques. During the past few years, crystals show decreasing concentration of impurities and better homogeneity of material properties. Substrate alloyed with zinc ($Cd_xZn_{1-x}Te$) shows higher uniformity of grown crystals, leading to easier production of large volume detectors. The most successful ones are [1]:

Vapour growth methods are based on the *Basic Bridgman* (BBM). This method involves the movement of a crucible containing the melt through a furnace designed to provide a desirable temperature profile. The furnace may be either vertical or horizontal. The crucible may be transported through the heater, or the crucible stationary with a moving heater, or alternatively, both stationary and the temperature profile altered by a programmed temperature controller. Most used modification s of BBM are *High Pressure Bridgman method* (HPB) and the *Low pressure Bridgman*. *Travelling heater method* (THM) is probably the most often used method of the CdTe / CdZnTe crystals growth used by commercial vendors, such as ACRORAD [2] and REDLEN [3]. In this method, the crystals grow from tellurium solution. The melting point of is usually set to 650°C by control of Cd to Te ratio. A moving RF heating coil is used to melt a narrow region of the crystal and as a segregator of impurities, which are pushed to the ends of the ingot.

CdTe crystallises into Zinc-Blende structure, which is a combination of two face-centred cubic lattices shifted to each other by Miller indices (¼, ¼, ¼). Such structure makes growth of CdTe / CdZnTe is much more difficult than it is for Si. Complicated crystal arrangement result into more frequent lattice defects. Probably the most common crystal defects are Cd vacancy V_{Cd} that acts as an acceptor due to missing electrons from the Cd atom. This defect is compensated by doping with Cl, In and others. Te_{Cd} is the Te antisite that has the opposite effect from V_{Cd} and acts as a donor. Beside lattice defects, charge transport and spectroscopic performance is also limited by macroscopic defects like *Dislocation networks*, which are result of thermal stress during solidification and cooling down. *Grain boundaries* can be formed during crystal growth at high temperature gradients or high growth speeds. Normally, the grain boundaries are introduced at the very early stage of crystal growth when the nucleation of numerous grains appears, or resulting from the instabilities at the growth interface**.** *Te inclusions / precipitates* generally are originated from the morphological instabilities at the growth: Te-rich melt droplets are captured from the boundary layer before the melt interface.

2.2 CONTACTS

Metallization of the crystals have also crucial effect on the detector performance. The nature of interface formation between CdTe/CdZnTe and metal results in formation of Ohmic or Schottky contacts. Improper interface reactions often result into degeneration of the contact. This can lead to lowering of rectification efficiency for Schottky contacts and for all cases, creation of trapping centers and sources of additive noise in the detector system. On the other hand, some interfacial layers can be beneficial: CdTe detectors based on homoepitaxial p–i–n diode structures, in which the intrinsic part is a high-resistivity (detector-grade) bulk crystal, while the n- and p-doped ones are homoepitaxial layers, should be able to show much lower values of the dark current [4].

To create an ohmic contact on a p-type CdTe, metal with work function higher than 5.97 eV is needed. Nevertheless, metal with work function higher than 5.97 eV does not exist. Near ohmic contacts on p-type CdTe are created by electroless deposition of Pt or Au and behave as the tunnelling contacts. Most frequent metals used to create Schottky contacts on p-type CdTe are In, Al, Ni. Cu is often used as a back contact for CdTe/CdS solar cells. However, work function of CdTe differs by its surface conditions, such as non stoichiometry, presence of oxides and it is difficult to obtain the work function by conventional analysis methods. Furthermore, Te-terminated or Cd-terminated side of (111) oriented crystal show differences in electrical behaviour of the contacts since Te-face is more conductive and has more n-type nature [3].

2.3 SURFACE

After mechanical cutting of the crystal from ingot, mechanically damaged layer is removed by grinding. In most cases, Al_3O_3 or B_4C grits are used, since diamond-based grids are too hard and leave deep mechanical scratches on the surface. This procedure is followed by fine free abrasive polishing. Al_2O_2 powders are most frequently used in a few steps with decreasing diameter of grain of the powder, typically from 10 μm to 0.3 μm. Intermediate procedure between mechanical and chemical processing is chemo-mechanical polishing. It is performed by using a polishing member made from soft natural or synthetic tissues, on which the etchant solution or suspension containing the etchant and abrasive particles is supplied [5]. After mechanical processing of the surface, the mechanically damaged and oxidised layer is still present. This layer is removed chemically. The most widely used solution is the solution of elemental bromine in organic and inorganic solvents. Such mixtures polishing properties and their etching rate are limited by the diffusion stages of heterogeneous properties and their toxicity. Such treated substrate is, however, Te rich [6] and contaminated by bromine. CdTe treatment using Br solution in CH_3OH leads to formation of a layer with an increased concentration of cadmium vacancies [7]. Beside chemical methods, “dry” methods can be applied. Plasma etching or ion bombardment are involved in these processes. Ar, H_2, O_2, CH_4

and their mixtures are used for plasma processing. Ar/H_2 plasma treatment seems to be the most promising for CdTe. Exposure to low flows (~1.5 sccm) succeeded in removal of carbon based organic residuals, removed excess Te from the Br-MeOH etched surface [8].

2.4 NOISE

Noise properties, as a result of unwanted electric signal fluctuations in time, are very important parameter that seriously limits manufacturing X-ray semiconductor detector with good spectral resolution and fast response. Determination of the noise sources and its neutralization is important for improved performance of the detector.

Not only manufacturing quality of the device has impact on the noise properties. Cooling of the detector loweres noise and leakage current, bring complications into final device design, increase power consumption and is bulky. 1/*f* noise is dominant for devices that operate at low frame rate [9] or for X-ray detectors with long collection time, understanding the mechanism of 1/*f* noise is crucial.

Beside the 1/*f* noise, there are other "basic" forms of noise, such as Johnson-Nyquist noise, Generation-Recombination noise, and shot noise. Idealized subscription of each noise type on the detector system is shown in Fig. 2.1. Total noise of theX-ray detection system can be expressed as:

$$S_n^2 = S_{1/f}^2 + S_{1/f^2}^2 + S_{GR}^2 + S_{shot}^2 + S_{ph}^2 + S_{amp}^2, \qquad (1)$$

where $S_{1/f}^2$ is the 1/*f* noise, S_{amp}^2 is the amplifier noise, S_{1/f^2}^2 is the material defect relaxation noise, S_{GR}^2 is the Generation –Recombination noise, S_{shot}^2 is the shot noise and S_{ph}^2 is the photon noise.

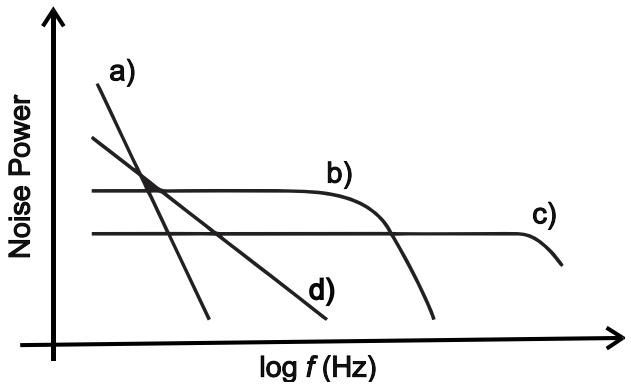

Figure 2.1: Typical subscription of noises sources in photodetector. a) Noise due to the relaxation of material defects (1/f^{-2}), b) Generation recombination noise or thermal relaxation noise, c) Shot noise or photon noise, d) 1/*f* noise.

Thermal (Johnson-Nyquist, White) noise is mainly caused by random, Brownian motion of the charge carriers and their collusions with the material atoms. This noise is present without applied voltage. Under zero voltage condition, under dark and

stable temperature, the power spectral density of thermal noise is expressed for short-circuit current as:

$$S_I = 4kT/R, \tag{2}$$

where k is the Boltzmann constant; S_I are noise spectral density of current. Sometimes, relation is multiplied by Δf as the bandwidth interval. This quantity is independent on material, has constant, "white" spectrum. The only quantities that influence thermal noise are temperature and electrical resistance R, respectively. The equivalent expression of eq. 2 for the open circuit voltage noise power spectral density S_U is

$$S_U = 4kTR. \tag{3}$$

Shot (Schottky) noise has its origin in discrete nature of electrons and holes, resulting in current shows burs-like character in time when travelling through the p-n junction or meta-semiconductor interface. In general, a condition for the shot noise is an existence of a potential barrier which has to be passed through by the charge carriers. The spectral density if the shot noise is given by the relation

$$S_I = 2qI, \tag{4}$$

where q is the elemental charge and I is the current flowing through the specimen.

Generation – Recombination noise (GR) is the result of presence of electrically active impurities or defects. For wide gap semiconductors, the GR centres are Shockley-Read-Hall type. Defects located closest to the midgap have the highest contribution to the GR noise [11]. Generated electron-hole pairs are pushed out in the depletion region by electric field. This current is known as the generation-recombination current. The basis of GR fluctuation current is based on fluctuation around equilibrium (state, when electron densities e and hole densities p are equal, i.e. $np = n_i^2$, where n_i is the intrinsic carrier concentration) of generated and recombined charge carriers between two conditions: When there are some excess carriers, $np > n_i^2$, the rate of recombination is higher than the rate of generation. Similarly, in the case of lack of carriers, $np < n_i^2$, the generation rate becomes higher than the recombination rate [12]. Spectrum of GR signal is given by formula [13]

$$S_i = \frac{S_N(\omega)}{N_0^2} = \frac{\overline{\delta N^2}}{N_0^2}\frac{4\tau}{1+(\omega\tau)^2}, \tag{5}$$

where ω is the angular frequency, N_0 is the average number of free carriers and δ is the variance of carrier number fluctuations. The spectrum of the fluctuations in eq. 5 is Lorentzian type with two parameters: the relative variance of number fluctuations and the lifetime of charge carriers.

Beside thermal, shot and GR noise, $1/f$ noise appears in semiconductor. Its exsitence has been reported intredisciplinary – in biological systems, music, finnacital market etc. General origin of $1/f$ noise is still not understood. $1/f$ noise dominates at low frequencies, typically below 1 kHz. Apart from GR noise, the $1/f$ noise is weakly dependent on tmperature. For electronic systems, $1/f$ noise is closely

linked with crystallographic defects, deep levels and with the quality of the interfaces. Among numerous models, the basic ones are:

McWhroter model that expect 1/*f* noise is a result of carrier's number fluctuation. In this model, the spectrum of 1/*f* noise is a superposition of Lorenyians with vast interval of relaxation times. This model seems to be acceptable for degenerative semiconductors and heavily oxidised surfaces. The resulting spectrum is given as superposition of *N* generation-recombination Lorezian fractional spectra with vast range of relaxation times within the limits τ_2 and τ_1.

$$S_N = \overline{4\Delta N^2}\int_{\tau_1}^{\tau_2} g(\tau_N)\frac{\tau_N}{1+\omega{\tau_N}^2}d\tau_N = (\overline{\Delta N})^2\frac{1}{f} \quad (6)$$

The power spectral density has white character up to the frequency $f_2 = 1/2\pi\tau_2$. After this limit, the power spectral density is proportional to 1/*f* in frequencies up to $f_1 = 1/2\pi\tau_1$. At higher frequencies than f_1, the proportion becomes $1/f^{-2}$.

Apart from McWhorter's model, *Hooge's model* assumes that the source of 1/*f* noise is a free carrier scattering. When a constant voltage is applied to a semiconductor resistor of resistance *R*, a fluctuating current *I*(*t*) is developed. This can only come about because the resistance *R*(*t*) of the device fluctuates [10].

$$\frac{\Delta I}{I} = -\frac{\Delta R}{R} \Rightarrow \frac{S_I(f)}{I^2} = \frac{S_R(f)}{R^2} \quad (7)$$

Clarke and Voss [10] proposed relation also dependent on resistance fluctuations that was irrespective of 1/*f* noise. $S_I(f)/I^2$ can be written as

$$\frac{S_I(f)}{I^2} = \frac{\text{const}}{f} \quad (8)$$

Hooge solved the question what is the content of the constant in eq. 8. He proposed that the missing parameter is the number of carries *N* and weakly temperature dependent material constant α. This empirical formula has form

$$\frac{S_i}{I^2} = \frac{S_u}{U^2} = \frac{S_R}{R^2} = \frac{\alpha}{Nf}. \quad (9)$$

3 EXPERIMENTAL RESULTS

3.1 LOCALIZATION OF THE LEAKAG CURRENT AND NOISE SOURCES IN CDZNTE DETECTOR SYSTEM

In this part of my work, the noise spectral density analysis is used to find the bottleneck of the detector system by means of evaluation of each detector part contribution to the total noise of the detector system. Furt his purpose, a detector equipped with the Guardring electrode that separates surface and bulk current was used.

Figure 3.1 presents the *I-V* characteristics of the examined detector. The picture on the left shows the *I-V* characteristics of the sample with disconnected guard ring electrode, whereas the picture on the right shows *I-V* characteristics with connected guard ring. Marking "contact A" and "contact B" indicates which of two contacts was biased in reverse mode, thus acting as rectifying.

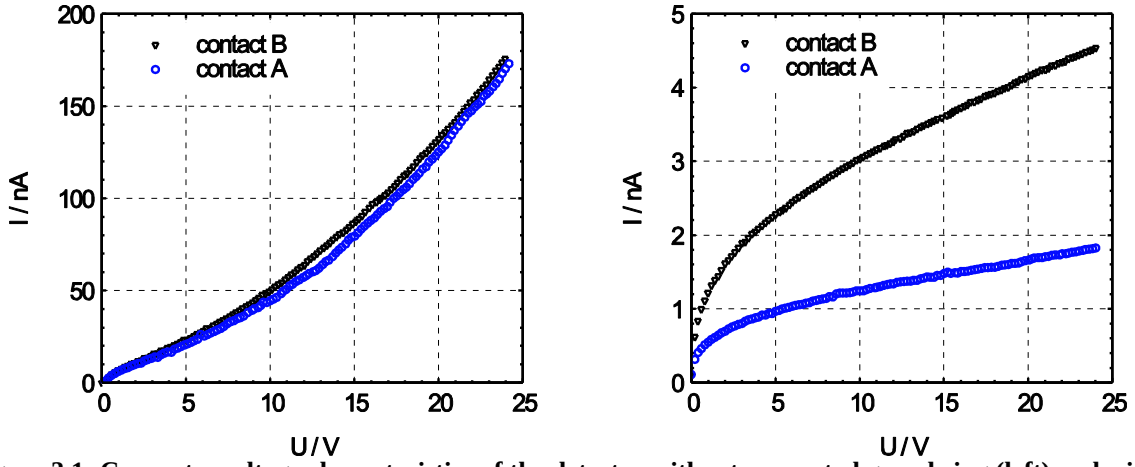

Figure 3.1: Current – voltage characteristics of the detector without connected guard ring (left) and with connected guard ring (right).

In the case of unutilized guard ring electrode (Fig. 3.1 left), I observed very symmetric behavior of both contacts, showing nearly identical rectifying properties. The characteristics bend upwards from the applied bias voltage U = 5 V due to the hole injection. If injection is not present, the increase of the current is due to thermally generated carriers linear with increasing applied voltage. In our case, the current increases with the second power of applied bias voltage, i.e. $I \sim U^2$. The *I-V* characteristics with connected guard ring electrode, shown in the right panel of Fig. 3.1, exhibit nearly two orders lower leakage currents. Compared with *I-V* characteristics of the detector with unutilized guard ring electrode, the *I-V* characteristics asymmetry is clearly visible. This asymmetry uncovers the difference of rectifying efficiency of each contact. At U = 25 V, contact A produces leakage current 1.95 nA, whilst the contact B has leakage current of 4.7 nA. This asymmetry points to the presence of higher concentration of imperfections at the area of the contact B.

Noise power spectral density Analysis: separation of noise sources

Figure 3.2 shows the noise spectral densities (PSDs) of detector with disconnected guard ring electrode. Solid black line in Fig. 3.2 (right) indicates the limit of the measurement apparatus. The key limitation is the thermal noise of the 100 kΩ load resistor.

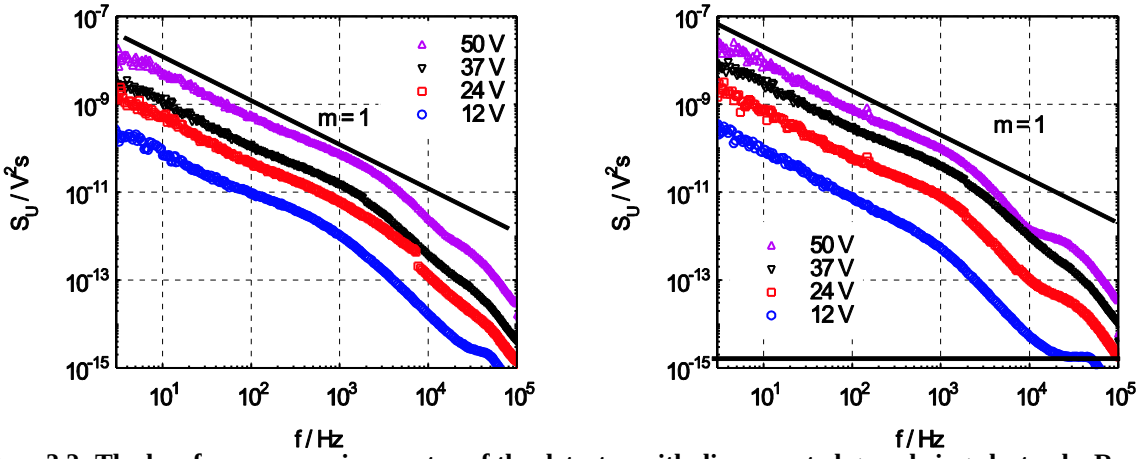

Figure 3.2: The low frequency noise spectra of the detector with disconnected guard ring electrode. Reverse biased contact A (left), reverse biased contact B (right).

The dominant $1/f^{\,m}$ noise, has parameter m close to 1. In the case of the reverse biased contact A and also for the reverse biased contact B, the shape of the spectra is similar. The reverse biased contact B shows slightly higher magnitude of the noise spectra that is in agreement with higher leakage current measured for the reverse biased contact B, as plotted in Fig. 3.1 (left). Nevertheless, the order of magnitude of the spectra is the has the same order (e.g.: 10^{-8} V^{2}s for U = 50 V and 10^{-10} V^{2}s for U = 12 V, measured at f = 10 Hz).

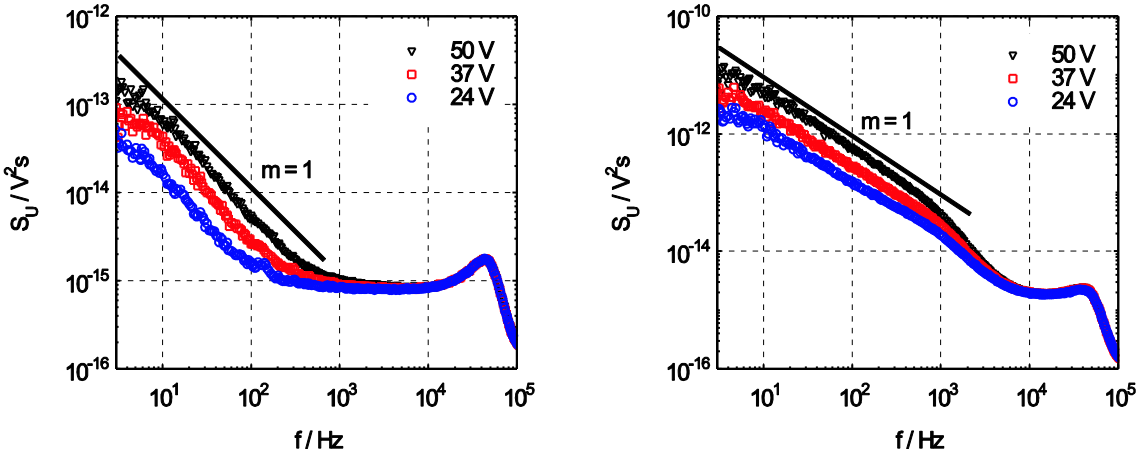

Figure 3.3: Low frequency noise spectra of the detector with connected guard ring electrode. Reverse biased contact A (left), reverse biased contact B (right).

The low frequency noise spectra of the investigated detector with connected guard ring are in Fig. 3.3. The slope of $1/f^{\,m}$ noise was the same like for the case of disconnected guardring, but with 2 orders lower magnitude. Detector bulk acts as the same source of excess noise, regardless on the bias polarity. Difference of magnitude of PSD is caused by an increased number of defects or imperfections in the area of the contact B. In case of disconnected of guard ring electrode, this behavior is masked.

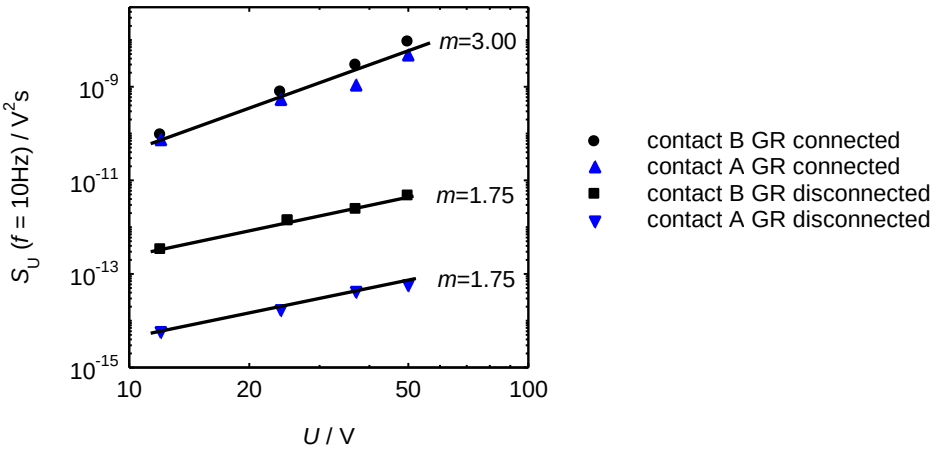

Figure 3.4: Dependence of power spectral density of the noise signal on the applied bias voltage at *f* = 10 Hz. Configurations with and without connected guard ring electrode are shown.

Figure 3.4 shows dependences of PSDs of the noise signal on the applied bias voltage The PSD of the noise signal generated by the surface increases with the power 3.091 (reverse biased contact A) and 2.873 (reverse biased contact B) with increase of the applied voltage. The PSD of the noise signal, generated by the bulk and contacts, rises with the power of 1.75 (reverse biased contact A) and the same value was obtained for the contact B. As can be seen, the increase of power spectral density with the applied voltage is independent on the bias polarity. Higher leakage current of contact B is the source of higher magnitude of its noise PSD.

This experiment showed that untreated detector surface was found as the bottleneck of detector system; it generates the highest contribution to the total leakage current of the detector. Surface acts as a conductive layer with high concentration of unwanted defects. The resulting *I-V* characteristics of the detector investigated with unutilized guard ring electrode mask the properties of the contacts and the bulk. The *I-V* characteristics with disconnected guard ring electrode for both bias polarities were very symmetrical and their shape indicates the presence of the carriers' injection, which leads to non-linearity of the *I-V* characteristics. After employing the guarding electrode, the contact asymmetry was revealed. The contact A showed better rectification efficiency and has lower contribution to the detector total additive noise. Utilization of the guard ring electrode caused two orders lower leakage currents and suppressed the total magnitude of the detector noise by 5 orders. Surface treatment (passivation or/and the guard ring electrode utilization) is beneficial processing step in CdTe based radiation detectors manufacturing to obtain a high quality spectroscopic radiation detector.

3.2 ELECTRIC FIEALD DISTRIBUTION AND NOISE EVOLUTION DURING THE POLARIZATION

The ionization of the deep acceptor by hole detraping and inducing a space charge buildup is most often reported as a responsible mechanism for polarization phenomena that happened on short time [14]. Such space charge builtdup influences noise properties and changes distribution of electric field in the sample. Dynamics of these processes was focus of this experiment.

3.2.1 Electric field distribution during polarization

The electric field distribution through the sample is obtained from the Pockels measurements in Fig. 3.5 represents the one-hour time decay of the internal electric field profiles in the studied sample when the bias is 50 V. It is observed that most of the bias is developed across the reverse biased contact of the structure.

Redistribution of electric field in time is apparent from Fig. 3.5. Right after biasing, the electric field is distributed towards cathode up to distance of 0.15 mm. As time goes on, the electric field distribution changes and grows in vicinity of the anode. As can be seen, the dead layer that has no electric field grows during the polarization. This effect reduces collection efficiency and spectral sensitivity of the detector since the carrier collection becomes more and more incomplete.

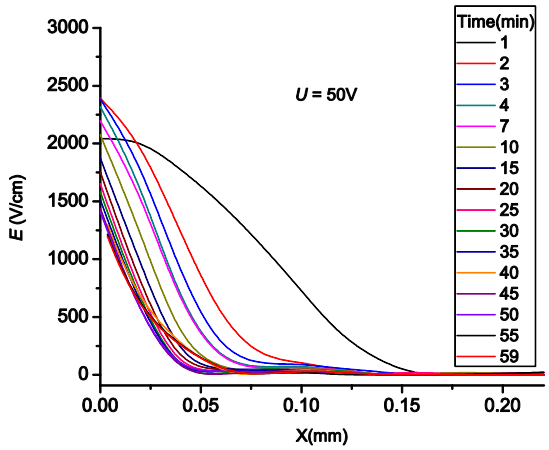

Figure 3.5: Distribution of the electric field with time through the sample acquired by the Pockels effect measurements.

Figure 3.6 (left) shows the evolution of the low frequency noise spectrum of the analysed detector in time. $1/f^{m}$ noise. At frequencies below 100 Hz, the slope m of the $1/f^{m}$ noise was very close to 1. The corner frequency of the $1/f^{m}$ noise with m = 1 gets lower during the polarization. This trend follows the $1/f^{m}$ noise with $m > 1$. The increase of the m parameter is caused by an increasing ratio of the generation-recombination processes in the total noise spectrum.

3.2.2 Evolution of noise during polarization

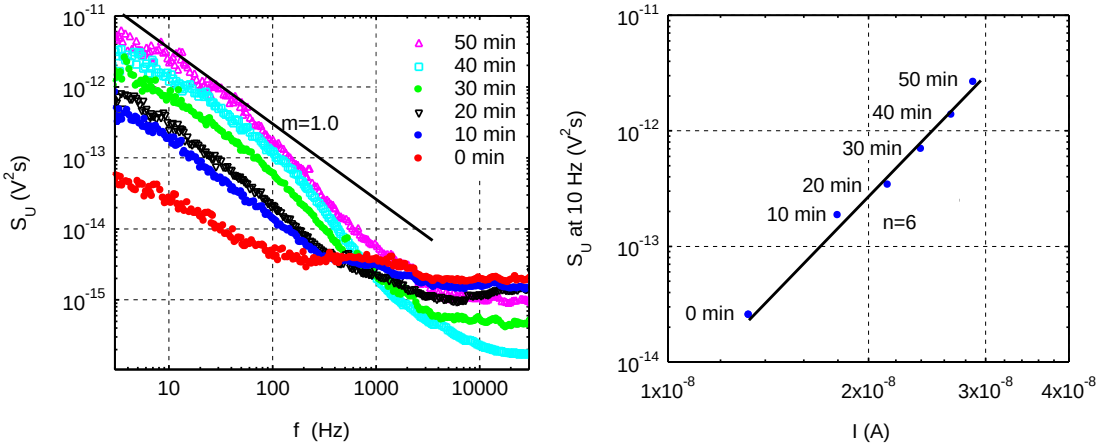

Figure 3.6: Noise spectral density evolution during polarization of the analyzed detector (left) and an increase of the noise spectral density with current. Applied voltage was 100 V.

At higher frequencies, the detector noise signal spectrum showed a shot noise shape, for which the slope m is typically 0. Later noise spectra, sampled 20, 30, 40 and 50 minutes after detector biasing, exhibit a decrease of shot noise spectral density level, which indicates a lowering effect of the shot noise during the polarization. For certain frequencies, e.g. at 100 Hz (t = 30 min) and at 70 Hz (t = 50 min), I observed an increase of the slope of the $1/f^{\,m}$ spectra from m = 1.4 (t = 20 min) to m = 2 (t = 50 min). As in case of the $1/f^{\,m\,=\,1}$ noise, the reason for this increase is a strengthened effect of the generation-recombination noise, which is typical for the trapping-detrapping process of carriers from energy states located in the band gap [15].

Figure 3.6 (right) has information about the dependence of the power spectral density on the leakage current during the polarization process. The increase is proportional to the power of n = 6 of the current. This finding is in contrast with theory, proposed by Hooge, which presumes an increase of the power spectral density with the square of the detector current. This disproportion can be described as follows: Hooge assumes a constant number of charge carriers in the system. This idea can be accepted in case of devices, where polarization is absent (MOSFETs devices etc.). In our case, after biasing the detector, charge carriers are detrapped from deep energy levels also in the space charge region forming a screen to the applied electric field. Carriers situated "in the shadow" of space charge become inactive for the overall electric charge transport of the detector. This mechanism causes an increase of the noise spectral density not only due to the current increase, but also due to the change of total carrier number in the detector system.

3.3 ANALYSIS OF THE CONTACT SYMMETRY AND ITS IMPACT ON THE LOW FREQUENCY NOISE.

This part of my work is aimed to analyse one of the key factors influencing detector performance: the symmetry of electrical parameters of the detector's

contacts with the same geometry. For this analysis, the *I-V* characteristics and additive noise of contacts are investigated.

Results of measurements on the investigated CdTe sample are shown in Fig. 3.7. The *I-V* characteristics are non-linear at low voltages and resistance of the sample increases with decreasing temperature. I have compared rectifying effect of each contact and its dependence on operating temperature. Fig 3.7 (left) shows detector with "poss" polarity. In this bias orientation and temperatures lower than 315 K, the detector shows good rectifying effect with linear reverse current increase with increasing bias

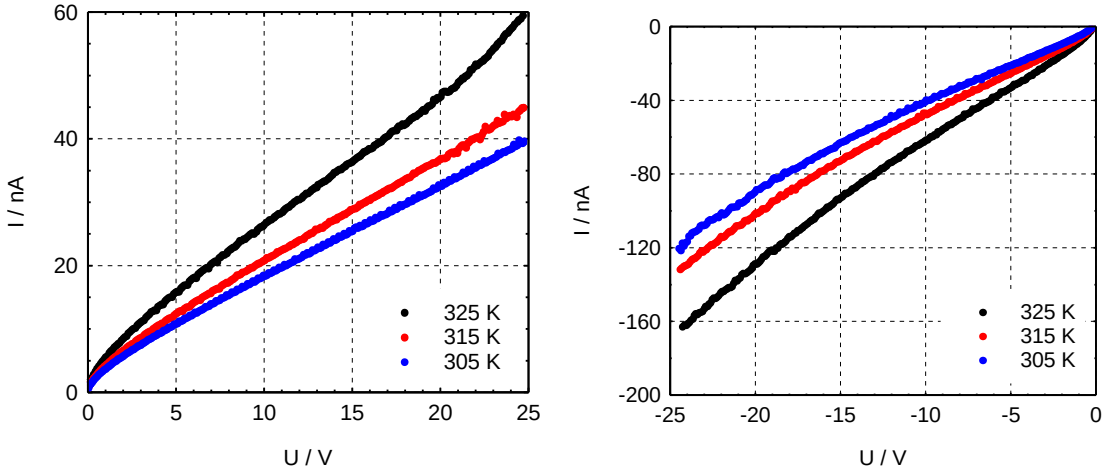

Figure 3.7: Current- Voltage characteristics of the "poss" (left) and of the "neg" (right) biased detector. Operating temperatures were 305 K, 315 K and 325 K.

In the case of "neg" polarity that is plotted in Fig 3.7 (right), the second contact acts as rectifying (Still, the "S" shape at the low voltages is present), but the leakage current is approx. three times greater than in case of the "poss" polarity. The rectifying effect is obviously worse than tin the "poss" polarity. Furthermore, *I-V*s for all temperatures show the tendency to become superlinear at higher biases.

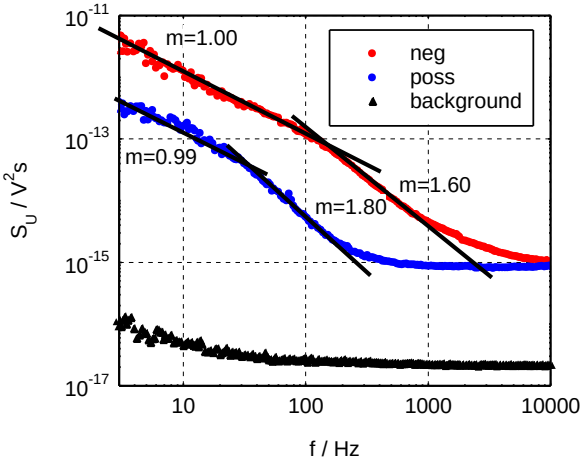

Figure 3.8:Comparison of the Low frequency noise spectra of the detector for both bias orientations. The applied bias was ±25 V, measured at temperature 305 K. Black line denotes noise background.

In Fig 3.8 are low frequency overall noise spectra of the investigated sample for both bias polarities. Applied voltage was 25 V. As can be seen, the reverse biased contact in the "neg" polarity shows three orders higher magnitude of detector's additive noise spectral density. For the "neg" polarity, change of the $1/f^{m}$ noise spectrum slope to higher value $m = 1.60$ at 100 Hz can be seen. In case of the "poss" polarity, the spectrum slope changed to 1.80 from 30 Hz. The non-uniformity of the slope m among both spektra is caused by different distribution of traps / defects in M-S interfaces of each contact. I have conducted the same analysis as in Section 3.1, i. e. received the increase of the noise PSD with the applied voltage. The results showed that the faulty "neg" reverse biased contact shows higher increase of the noise power spectral density than the "poss" one. The well rectifying concact showed increase of PSD with ideal power of 2, whereas the "neg" contact showed the increase with the exponent of 3.6.

To sum up, the investigated sample showed serious asymmetry of electrical parameters, caused by the difference between qualities of each contact. The measurement results points to presence of higher concentration of defects in metal-semiconductor contract area, which lead to the barrier non-uniformity and increase of the leakage current. The contact imperfection also causes additional noise of the detector, significantly increasing with the applied bias voltage.

3.4 INVESTIGATION OF THERMAL STRESS EFFECT ON CDTE DETECTORS

Motivation of this part is the fact that one of typical features of CdTe and CdZnTe is irreversible changes of the detector parameters that start at relatively low temperatures around 400K. The nature of irreversible changes in the detector structure and the effect of them on not only electrical, but also structural properties of the CdTe detector system is subject of the following chapter.

3.4.1 Analysis of the effect of thermal stressing on charge transport properties

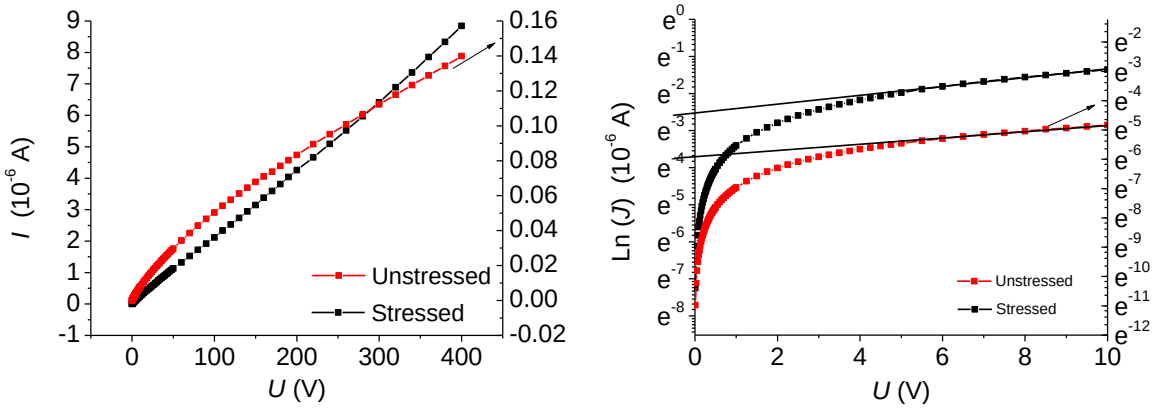

Figure 3.9: *I-V* characteristics of stressed and unstressed samples (left). Right picture: Transformed ln(*J*)-*V* curves for low biases of each sample.

Fig 3.9 shows comparison of the *I-V* characteristics from (left) 0 V to +400 V, and (right) are transformed *J-V*s from 0 V to +10 V. My previous measurements showed symmetry of the characteristics biased with the negative polarity. Resistivities obtained from the *I-V*s at bias voltage < 0.2V were $\rho = 1\times10^{9}$ Ωcm for the unstressed sample and of $\rho = 4\times10^{6}$ Ωcm for the stressed sample. Remarkable change can be seen from comparison ofthe shapes both characteristics. Unstressed detector shows typical S shape of the *I-V* characteristic, which is given by rectification effect of the contact ($R_c > R_s$), whereas the stressed detector shows linear, ohmic character ($R_c < R_s$).

The current responses of both investigated devices at low bias voltages (0 - 10V) transformed from the *I-V* curves into ln(*J*)-*V* curves as can be seen at Fig.3.9 (right). The current density *J* for Schottky contacts is given by equation [16]

$$J = J_s \exp\left(\frac{qV}{nkT}\right)\left[1-\exp\left(\frac{qV}{kT}\right)\right], \qquad (10)$$

where J_s is the saturation current given by

$$J_s = A^* T^2 \exp -\frac{q\phi_B}{kT}, \qquad (11)$$

where *A** is the Richardson constant for CdTe and is equal to 120 $Acm^{-2}K^{-2}$, *q* is the electron charge, V the applied bias voltage, *k* is the Boltzmann's constant, *T* the temperature 300 K, ϕ_B the Schottky barrier height, and J_s the saturation current density obtained from intercept of the linear part ln(*J*)-*V* curves at zero voltage, as shown in Figure 3.9 (right). From all known values of above mentioned quantities, the Schottky barriers heights are calculated as:

$$\phi_B = \frac{kT}{q}\ln\left(\frac{AT^2}{J_s}\right). \qquad (12)$$

The received values of the Schottky barriers are 0.786 eV for the degenerated device and 0.867 eV for the undegenerated detector, respectively. I assume this change to thermally activated diffusion of Au into the CdTe bulk. Increased concentration of In in vicinity of M-S interface and permanent depletion of Cd entrenches this effect. Au locally dopes the sample, which changes the electrical properties of the interracial layer. This change in the electrical properties results in reduction of the barrier height. This conclusion is confirmed by the XPS depth profile of Au shown in section 3.4.2. I have to note that the results given by eq. 10 should not completely describe reduction of the Schottky barrier height, since the parameter *A** is given as

$$A^* = \frac{4\pi m_e^* k^2 q}{h^3}, \qquad (13)$$

where the electron effective mass m_e^* ~ 0.13 ×free electron mass m_0 is material dependent. As revealed by XPS, the M-S interface of investigated samples is a very inhomogeneous heterostructure and contains mixture of purely metallic or mixed forms of Cd, Te and its oxides and electrically active Cl. This brings serious

uncertainty for M-S electrical properties analysis based on the regular charge transport models.

3.4.2 Structural investigation: XPS depth profiling of the M-S structure

This chapter is dedicated to analyse properties of M-S junctions of the samples before and after thermal stressing by description of changes of their elemental depth profiles. From comparison of figures 3.10 and 3.11 it is clearly apparent structural change caused by increased operating temperature of the semiconductor crystal. M-S interfaces of both samples were Te-rich. The non-stoichiometry for the case of unstressed detector shows was present up to 600 s of sputtering.

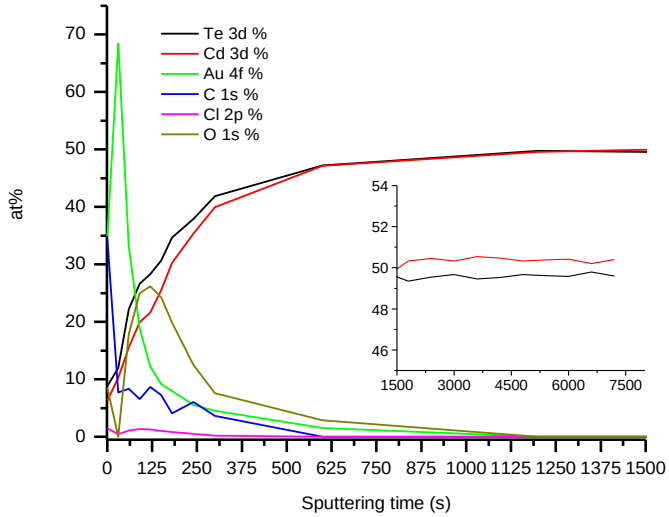

Figure 3.10:XPS depth profile of the M-S interface of the unstressed sample.

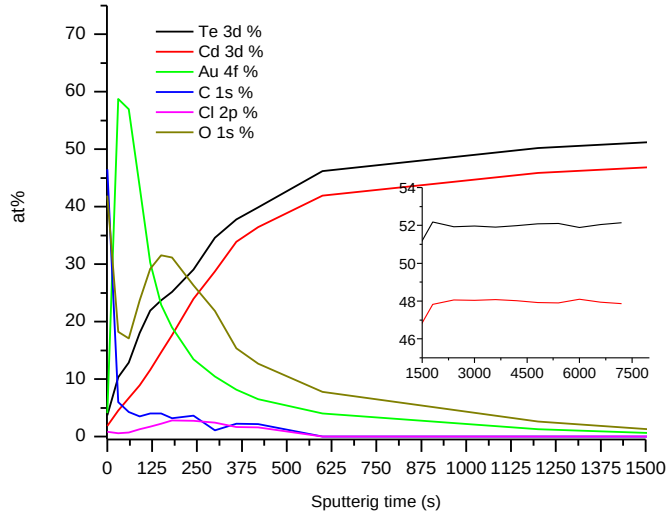

Figure 3.11:XPS depth profile of the M-S interface of the stressed sample.

Even more significant deviation from stoichiometry is remarkable for the stressed detector. For both samples, highest deviation of non-stoichiometry was measured

after 120 s of sputtering. The stressed sample showed Te / Cd ratio 1.893, whereas the unstressed sample was Te rich with ratio of 1.310. In both cases, the maxima of non-stoichiometry are linked with the highest concentration of oxygen. Measured values of O atomic concentrations are 31.53 % (stressed sample) and 26.22 % (not stressed sample). Distinctive, more than 5% difference between oxygen in favour of the stressed sample points to adsorption of oxygen at higher temperatures.

Insets in the Fig. 3.10 and Fig.3.11 show Cd/Te atomic concentrations at higher sputtering times. The only detected elements by XPS were purely metallic Cd and Te. The unstressed sample show nearly stoichiometric ratio of Cd and Te deeper in the crystal bulk. The atomic concentration difference within 0.2 % can be attributed to measurement error of the used instrumentation. On the other hand, the stressed sample shows significant depletion of Cd in its volume. At all XPS scans at longer sputtering times, The Te/Cd ratio had constant value of 1.085. I can omit the effect of large (> 1 μm) Te inclusions since the sputtered area was large enough. From these apparent differences revealed by XPS, I can conclude that ambient temperature higher than 400 K cause release of Cd from the crystal structure and it is the main effect of irreversible change of the bulk properties as a consequence of thermal stress of the detector

Another feature is enhanced diffusion of Au into the detector bulk. For the case of the unstressed detector, the Au photoemission signal disappeared after 1200 s of sputtering, whereas gold signal was presented up to 1800 s for the case of stressed detector. Evolution of Au concentration decrease with depth was much steeper for unstressed sample than for the stressed one, put integration of both curves yield the same results. For both sample, the presence of oxygen, which is hand-in-hand with existence of TeO_2 in the structure is connected with presence of Au.

To analyse such small chemical shifts (binding energy variances are below 0.2 eV) I used different, less common method: Comparison of Cd 3d photoemission peaks possitions with atomic concentrations of sub-oxide chemical states of Te and atomic concentration of Cl in M-S interface of both samples. This relation is depicted in Fig. 3.12. This clearly justifies the existence of sub-oxide form of Te and the origin of binding energy shift of Cd, which is closely linked with existence of Cl, dissociated from $AuCl_3$. The reaction of $AuCl_3$ with the CdTe surface is described by the formula

$$4AuCl_3 + 6CdTe \rightarrow 4Au + 12Cl^- + 6Cd^{2+} + 6Te. \qquad (14)$$

Onwards, Cl reacts to cadmium chloride ($CdCl_2$ with binding energy 406.1 eV) with concentration below detection threshold of the XPS system, i.e. concentration < 10^{19} cm^3 (considering the atomic density of CdTe of approx. 10^{22} atoms / cm^3).

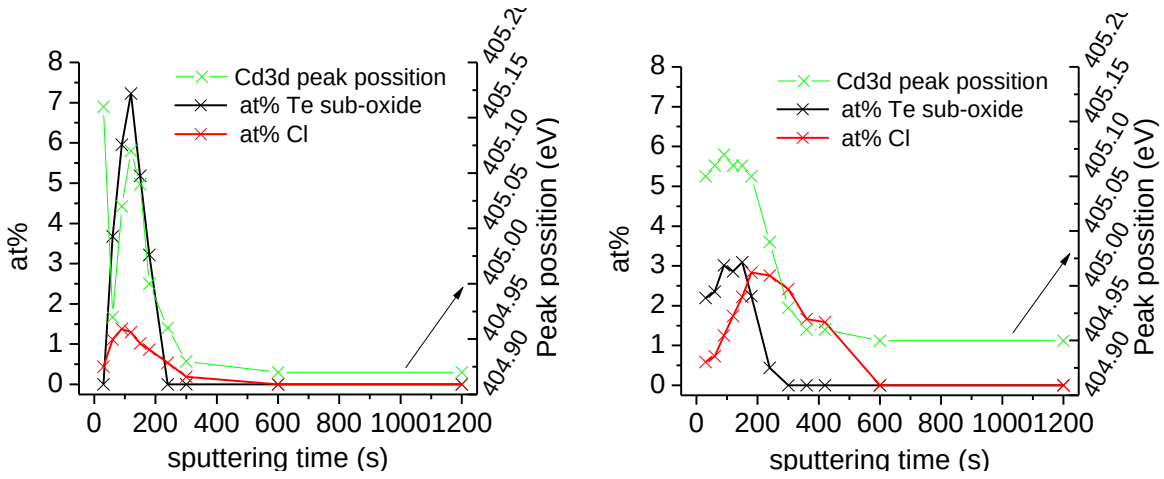

Figure 3.12:Comparison of chemical shifts of the Cd 3d photoemission peaks with the atomic content of Cl and Te sub-oxide. The unstressed sample is on the left.

Even though $CdCl_2$ is not clearly detected by XPS, a shift of the Cd 3d 5/2 peak towards higher binding energies can be observed. Te partially or segregates into pure metal during deposition or oxidize into TeO_2 delivered from the aqueous solution of $AuCl_3$, since $AuCl_3$ dissolved in water forms $H[AuCl_3(OH)]$ [17]. For both Cd and Te, volume of $AuCl_3$, which is (approx. 10 nm × contact area) is much smaller than the volume of CdTe crystal. Furthermore, from eq 14 can be clear that there is not enough oxygen for complete transformation of Te into TeO_2, leading to formation of the sub-oxide form of Te. Aqueous solution of $AuCl_3$ is initially neutral and decomposes gradually in time with separation of gold. Therefore, the $AuCl_3$ solution has ageing features and its actual chemical state has unneglectable influence on chemical composition of the M-S interface and reduces repeatability of of chemical / electrical parameters of the M-S interface.

Comparing depth profiles of the quantities depicted in Fig 3.12 for both samples, concentrations / Cd 3d photoemission peak positions are quite comprisable. Some distortion of distribution is visible for the stressed sample (Fig 3.12 right), showing less abrupt increase of concentration of sub oxide and $CdCl_2$. Constant binding energy shift approximately of 0.05 eV to higher energies, which is present for the Cd3d photopeak of the stressed detector among the whole scanning interval up to 7200 s (not shown), is a result of permanent deviation from stoichiometry (see Fig. 3.11). Higher atomic concentration of Cl and its unpredictable diffusion might be the reason of difficult reproducibility of contact deposition by aqueous solution of $AuCl_3$.

Figure 3.13 shows depth profile of concentration of Te chemical states. Three chemical states of Te were found. i.) Metallic form, ii) Te^{4+} (TeO_2) form and iii) sub-oxide form. Generally, sub-oxides are a class of oxides wherein the electropositive element or a radical is in excess relative to the “normal” oxides. [18] When the electropositive element is a metal, the compounds are sometimes referred to as metal-rich.

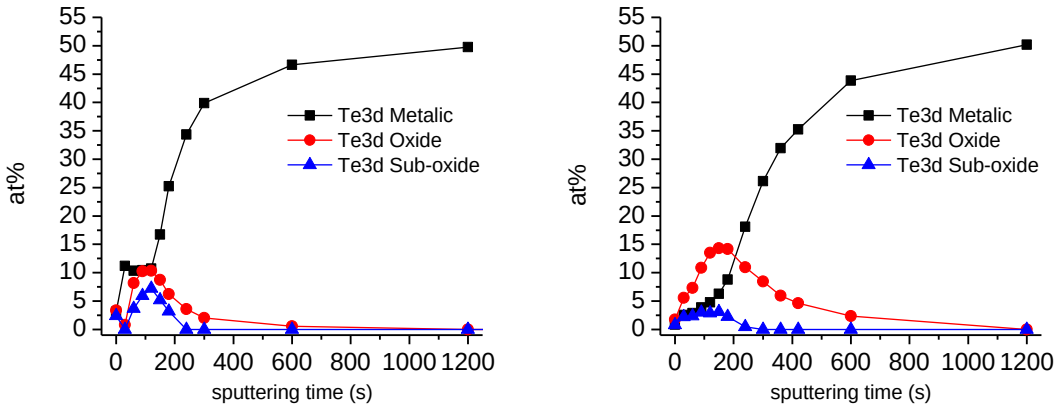

Figure 3.13:Depth profiles of atomic concentrations of Te in its metallic form, oxidized form and sub-oxide form. The unstressed sample is on the left.

Figure 3.13 confirms that diffusion of Te sub-oxide as a result of thermal treatment is negligible. On the other hand, different situation occurs for Te in its TeO_2 form. The stressed sample shows the presence of TeO_2 remarkably deeper in the sample bulk. After 1200 s of sputtering, TeO_2 is still detected with atomic concentration of 0.45 %.

3.5 INVESTIGATION OF THE EFFECT OF THE ARGON ION BEAM ON CDZNTE SINGLE CRYSTALS SURFACE STRUCTURAL PROPERTIES

Motivation of this part of my work was investigation of the surface by "dry" etching method, by argon ion beams. this experiment, I tried removal of mechanically and chemically damaged surface by relatively low doses of Ar^+ ions beam. Due to different structural properties, my aim is to remove the defective layer without modification of undamaged bulk volume of CdZnTe crystals. The analyses of the crystal structure after ion beam bombardment is conducted SEM, AFM and XPS.

3.5.1 SEM study of irradiated surface

Fig. 3.14(a) depicts the surface before ion bombardments. Even before irradiation, remarkable etch pits after Br-MeOH etching are visible. Similarly, as for some other etching solutions like Everson solution [19], it was reported that Br-MeOH, especially at concentration higher than 2% and with presence of light, has the tendency to uncover structural defects. Fig. 3.14(b) shows the detector surface after irradiation by a dose of 3.7×10^{15} Ar^+ ions/cm^2. Obviously, the randomly distributed etch pits are smoothened. More apparent features are dislocation-related lines. The single etch pits form cellular or polygonal arrangements. Such a structure is typically observed if the crystal is grown in a high temperature gradient where the dislocations are gathered around sub-grain boundaries [20, 21].

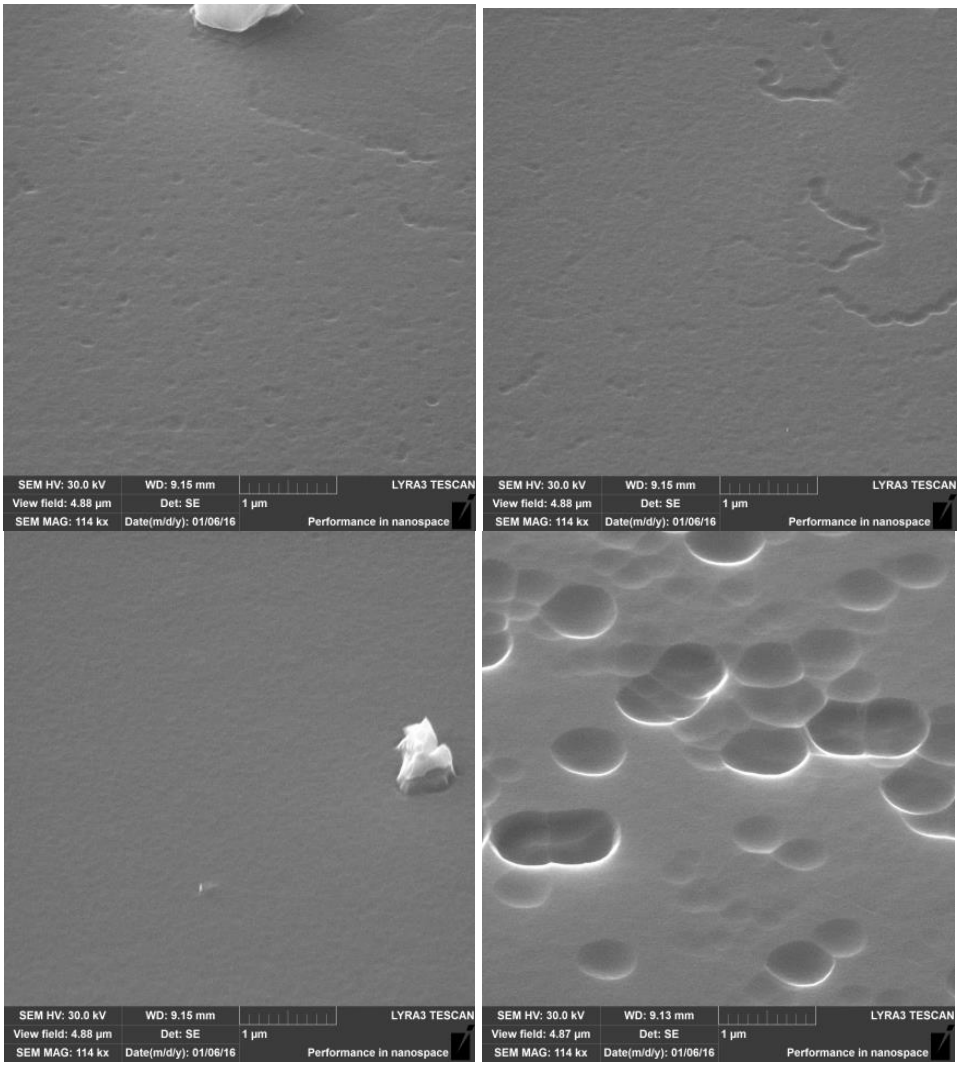

Figure 3.14: SEM micrographs of CdZnTe surface a) freshly etched before ion irradiation b) After Ar^+ ion fluence of 3.7 ×1015 Ar^+ ions / cm^2, c) 1.4 × 10^{16} Ar^+ ions / cm^2, and d) 2 × 10^{17} Ar^+ ions / cm^2

Surface exposed to fluence of 1.4×10^{16} Ar^+ ions/cm^2 in Fig. 3.14(c) shows complete vanishing of the shallow randomly distributed etch pits The surface seems to be reconstructed, no evidence of etch pits, dislocation networks or scratches from mechanical polishing are visible. The bright large volume artifact on the right-hand side of the picture was identified by EDS as a Te inclusion. The highest applied dose 2×10^{17} Ar^+ ions/cm^2 displayed in Fig. 3.14(d) caused significant change of the surface morphology. The irradiation caused craters as described for the previous case, with increased diameters to approx. 1 µm, covering most of the surface area. Herein I explain the nature of these: As a result of imperfect crystal growth, Te inclusions are randomly distributed in the crystal volume. The ion bombardment supplies energy to the crystal structure. Te clusters and dislocation patterns act as attractors for energy exchange. In other words, the energy is preferably given to buried metallic Te located just below the surface and the CdTe layer between the surface and Te cluster location is preferably removed.

3.5.2 AFM and XPS study of irradiated surface

Fig. 3.15(a) shows an AFM image of the just chemically etched surface. Its height is distributed homogeneously; no mechanical scratches; surface waviness is visible. After the dose of 3.7×10^{15} Ar^+ ions/cm^2, the surface firstly showed remarkable surface morphology change.

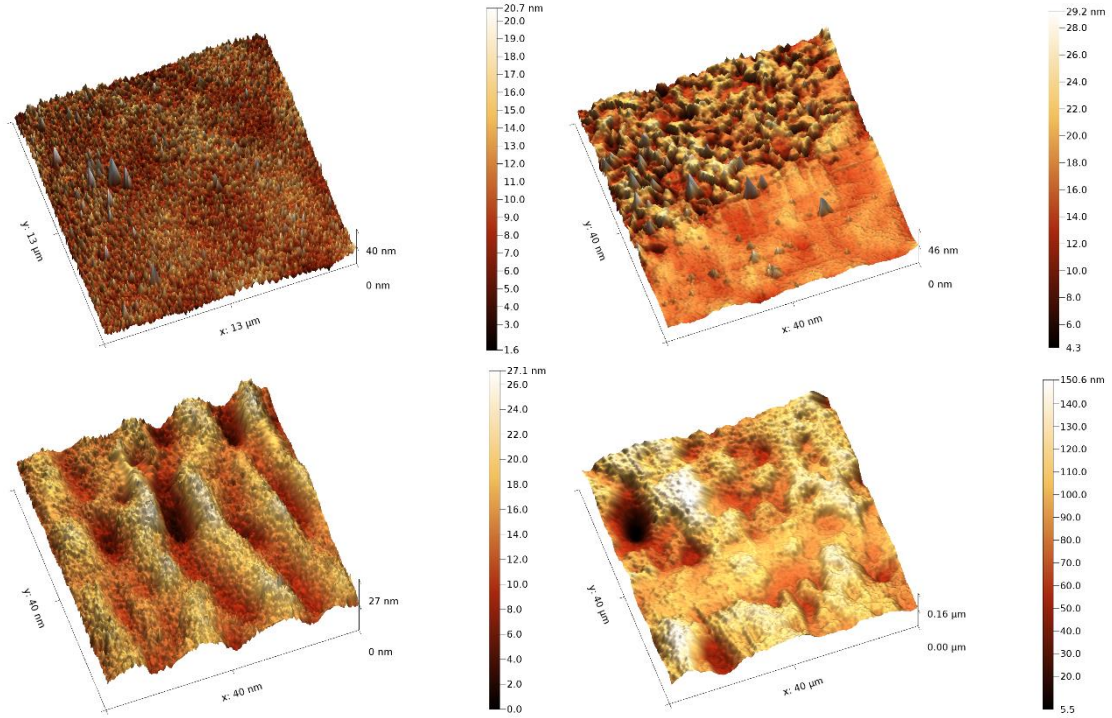

Figure 3.15: 3D AFM images of CdZnTe surface a) freshly etched before ion irradiation b) After Ar^+ ion fluence of 3.7 ×1015 Ar^+ ions / cm^2, c) 1.4×10^{16} Ar^+ ions / cm^2, and d) 2×10^{17} Ar^+ ions / cm^2

After the dose of 3.7×10^{15} Ar^+ ions/cm^2, the surface firstly showed remarkable surface morphology change. Two apparently different regions appear — a smooth one in the lower part of Fig. 3.15(b) and a very rough part in the top part of the picture. The rough part is mutually 15 nm deeper/lower penetrated than the plain of the smooth surface. I assume that creation of these regions is the result of an incomplete removal of mechanically damaged surface, which thickness can be from tens of nm to several µm. The smooth area has more porous-like structure than the unirradiated surface. Fig. 3.15(c) depicts the surface morphology after the dose of 1.4×10^{16} Ar^+ ions/cm^2. For this ion dose, the SEM micrograph in Fig. 3.14(c) showed best morphology. Similar results come from the AFM. However, waviness of the surface is apparent. Our search among the whole crater did not result in finding such heterogeneous surface like in the previous two cases. The surface shows very high smoothness without any steep peaks (dust, residuals on the surface), but apparent waviness with signs of a new crater generation. Nevertheless, the depth of these craters did not exceed 13 nm below the valleys originated by the ion irradiation. Finally, Fig. 3.15 (d) represents AFM data for the dose of 2.0×10^{17} Ar^+ ions/cm^2. Such a dose caused conversion of the smooth surface of the

sample to a heavily eroded one with randomly distributed pits on the surface, which are up to 110 nm deep.

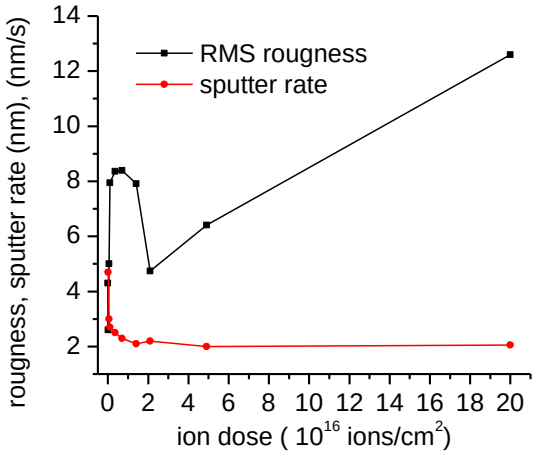

Figure 3.16:Dependence of the surface RMS roughness (squares) and the sputter rate (dots) on the Ar+ion dose.

Fig. 3.16 shows relation of the surface the RMS roughness (squares) and the sputter rate (dots) on ion dose. Sputter rates were calculated from difference of medium depths of the craters generated by the previous, lower dose and differences of sputtering times between lower and higher dose. Roughness of the unsputtered surface was 4.31 nm. After ion dose 1×10^{14} ions/cm^2, the surface roughness decreased to 2.6 nm. This was followed with the change of etch rate from 4.7 nm/s to 3.0 nm/s. The reason of such a significant change of both parameters is removal of carbon contamination on the surface, a residual from methanol that was used to rinse away the Br-MeOh etchant as reported in other studies, e.g. [22]. This situation is confirmed by XPS mapping of the C1s photopeak. The Te-rich layer, which also favors the higher sputter rate, originates from chemical etching and has a thickness of about 2 nm [23]. The fluence of 1×10^{14} ions/cm^2 was sufficient to remove the Te-rich layer, since sputtering time to remove a 2 nm thick layer is 400 ms. Sputter rates of higher fluences monotonously decreased to the value 2.2 nm/s (for fluence 1.4×10^{16} ions/cm^2), which corresponds to an approx. 145 nm deep crater, measured by profilometer. For the other higher doses, the sputter rate remained constant.

The surface roughness has remarkably increased just after the first “cleaning” fluence 1×10^{14} ions/cm^2 and had approximately the same value around 8 nm for doses from 1×10^{15} to 1.4×10^{16} ions/cm^2. For the value 2.1×10^{16} ions/cm^2, the roughness of the surface dropped to the value 4.74 nm, but as mentioned previously, extended surface waviness appeared. Surface erosion caused by higher irradiation doses caused increasing surface roughness ending at 12.6 nm for the fluence 2×10^{17} ions/cm^2. 1.3 μm of the surface was removed by this dose.

Conducted XPS analysis revealed that the relative concentration of Te /(Cd + Zn + Te) that shows that the stoichiometry of the surface did not show remarkable changes during sputtering - no preferential removal of eider Cd (Zn) or

Te happened. Preferential removal is related to structural defects buried beneath the surface. Argon ion irradiation has a similar feature as Br-MeOH etching, i.e. surface smoothening and improve its condition, followed by uncovering structural defects at higher doses / etching times. Found best dose of approx. 10^{16} Ar^{+} ions resulted in smooth surface. Such dose showed no damage signs, like irradiated surface waviness, preferential milling of either Te or Cd(Zn).

4 CONCLUSION

In my work, I employed more than eight analytical methods in order to investigate detectors features at various stat of quality. The first part of the work was dedicated to analyse samples by additive noise analysis, *I-Vs*, current stability and electric field distribution. Also, I separated noise sources of the detectors. My findings from this part are:

- Surface leakage current is the dominant source of noise and has highest contribution to leakage currents of the detector system[a1]
- From the Pockels effect measurements, space-charge build-up appears after the detector biasing. This result in creation of inactive, dead layers with zero electric field
- Polarization influences noise properties of the detector system. I observed increase of the $1/f$ noise in time with much higher exponent than two with increasing current. The reason of much steeper increase of the noise with increasing current is screening effect of the space charge and changes of spatial distribution of charge carriers in the bulk and, especially in vicinity of contacts. On contrary, polarization supresses the shot noise of the detector [a2].
- Improper contacts deposition results in expectable higher leakage currents. Additive noise analysis showed that the most significant change is the how big is the increase of the $1/f$ noise spectral density with applied voltage.
- Long-time exposure of the detector to temperatures higher than 400 K causes its irreversible degradation. This leads to higher leakage current and, again significantly higher increase of $1/f$ noise with applied bias voltage.

To generalize above mentioned facts, a good detector from should have these features:

- Low leakage current that, emphasized by rectification effect of Schottky contacts should have resistivity equivalent to 10^{11} Ωcm. At higher voltages, the characteristics should be linear, without any signs of superlinearity, cause by tunnelling etc.
- $1/f$ noise spectrum should have constant value of m in the whole frequency band, where $1/f$ noise applies. The value of m should be around unity. Variability of m in $1/f^{m}$ noise spectrum is a sign of dominating defect level. Opposite case appeared in all defective states of samples, including developed space charge.

- Increase of the value of $1/f^{m}$ noise spectral density with power of two with increasing bias voltage / leakage current. Higher values were typical for all defective states of samples, including developed space charge.
- Position of the$1/f^{m}$ noise corner at as low frequencies as possible. Unfortunately, higher sensitivity and higher bandwidth of the signal sampling is needed. This will be focus of my work for the future.

The second part of my work dealt with structural and morphological properties of M-S interface of a detector grade detector and irreversively degraded one by exposure to high operational temperatures for long time. For my investigation, I used advanced analytical methods: XPS, AFM, SEM, Scanning Auger Microscopy X-ray Diffraction and Secondary Ion Mass Spectroscopy as tools for the analysis.

The XPS results showed that the borderline between CdTe and Au is not abrupt, but with signs of diffusion of Au into the crystal bulk. The Au 4f photoemission peak was not shifted and gold is present only in its purely metallic form. The O 1s peak was detected during the existence of Au in the XPS spectrum. Even more interesting behavior showed Cd and Te. During depth profiling Cd showed very slight < 0.2 eV shift from its metallic state. This generally known fact makes difficult to distinguish oxidation state of Cd by XPS. Therefore, I carried out unconventional and yet not published comparison of Cd 3d photoemission peaks positions with the atomic concentrations of sub-oxide states of Te and atomic concentration of Cl in M-S interface. This showed that the existence of Te sub-oxide and the slight shift of is linked to presence of Cl in the spectrum. After disappearance of Cl from the XPS spectrum, only Te^{4+} (TeO_2) and metallic Te were found. After vanishing of the Te^{4+} state, the Cd/Te ratio attained stoichiometry, i.e. from Te-rich to the ratio of Te/Cd = 1. Diffusion depth of $H[AuCl_3(OH)]$ defines the thickness of bilayer between Au and CdTe. This bilayer has serious effect on the detector performance. It is a distorted structure, where CdTe is strongly dissociated, because Cd reacts primarily with Cl and Te forms TeO_2 and some Te is left in its metallic form. Such situation leads to detection of sub-oxide form of Te by XPS. Comparison of the data for stressed and unstressed sample showed permanent depletion of Cd for the case of stressed sample. Otherwise, chemical properties in M-S interface were quite similar, but the stressed detector showed more gradual depth profile of O, Cl and Au, pointing at that thermal stress cause enhanced diffusion of these elements into the bulk. I find the depletion from Cd as the most important result of thermal stress of the detector. This serious structural change results in different morphology and nanopatterning sputtered areas.

The last part of my work was focused on finding the best dose of Ar^{+} ions for the surface bombardment. The aim was reconstruction of the sample surface that was etched in Br-MeOH solution. This required minimal additional damage of the surface. Found best dose of approx. 10^{16} Ar^{+} ions resulted in smooth surface. Such dose showed no damage signs, like irradiated surface waviness, preferential milling of either Te or Cd(Zn) [a3].

Abstract

Because of demands from space research, healthcare and nuclear safety industry, gamma and X-ray imaging and detection is rapidly growing topic of research. CdTe and its alloy CdZnTe are materials that are suitable to detect high energy photons in range from 10 keV to 500 keV. Their 1.46 -1.6 eV band gap gives the possibility of high resistivity (10^{10}-10^{11} Ωcm) crystals production that is high enough for room temperature X-ray detection and imaging.

CdTe/CdZnTe detectors under various states of their defectiveness. Investigation of detector grade crystals, crystals with lower resistivity and enhanced polarization, detectors with asymmetry of electrical characteristics and thermally degenerated crystals were subject of my work in terms of analysis of their current stability, additional noise, electric field distribution and structural properties. The results of the noise analysis showed that enhanced concentration of defects resulted into change from monotonous spectrum of $1/f$ noise to spectrum that showed significant effects of generation-recombination mechanisms. Next important feature of deteriorated quality of investigated samples was higher increase of the noise power spectral density than 2 with increasing applied voltage. Structural and chemical analyses showed diffusion of metal material and trace elements deeper to the crystal bulk. Part of this work is also focused on surface modification by argon ion beam and its effect on chemical and morphological properties of the surface.

Abstrakt

Poptávka ze strany vesmírného výzkumu, zdravotnictví a bezpečnostního průmyslu způsobila v posledních letech zvýšený zájem o vývoj materiálů pro detekci a zobrazování vysokoenergetického záření. CdTe a jeho slitina CdZnTe. jsou polovodiče umožnují detekci záření o energiích v rozsahu 10 keV až 500 keV. Šířka zakázaného pásma u CdTe / CdZnTe je 1.46 -1.6 eV, což umožňuje produkci krystalů o vysoké rezistivitě (10^{10}-10^{11} Ωcm), která je dostačující pro použití CdTe / CdZnTe při pokojové teplotě.

V mé práci byly zkoumány detektory CdTe/CdZnTe v různých stádiích jejich poruchovosti. Byly použity velmi kvalitní spektroskopické detektory, materiál s nižší rezistivitou a výraznou polarizací, detektory s asymetrií elektrických parametrů kontaktů a teplotně degenerované vzorky. Z výsledků analýzy nízkofrekvenčního šumu je patrný obecný závěr, že zvýšená koncentrace defektů způsobí změnu povahy původně monotónního spektra typu $1/f$ na spektrum s výrazným vlivem generačně-rekombinačních procesů. Další výrazná vlastnost degenerovaných detektorů a detektorů nižší kvality je nárůst spektrální hustoty šumu typu $1/f$ se vzrůstajícím napájecím napětí se směrnicí výrazně vyšší než 2. Strukturální a chemické analýzy poukázaly, že teplotní generace detektorů způsobuje difuzi kovu použitého při kontaktování a stopových prvků hlouběji do objemu krystalu. Část mé práce je věnována modifikaci povrchu svazkem argonových iontů a jejímu vlivu na chemické složení a morfologii povrchu.

References

[1] SCHLESINGER, T. E., J. E. TONEY, H. YOON, E. Y. LEE, B. A. BRUNETT, L. FRANKS and R. B. JAMES. Cadmium zinc telluride and its use as a nuclear radiation detector material. *Materials Science and Engineering: R: Reports*. 2001, **32**(4-5), 103-189. DOI: 10.1016/S0927-796X(01)00027-4. ISSN 0927796x.

[2] SHIRAKI, H., M. FUNAKI, Y. ANDO, S. KOMINAMI, K. AMEMIYA a R. OHNO. Improvement of the Productivity in the THM Growth of CdTe Single Crystal as Nuclear Radiation Detector. *IEEE Transactions on Nuclear Science*. 2010, **57**(1), 395-39. DOI: 10.1109/TNS.2009.2035316. ISSN 00189499.

[3] CHEN, H., R. B. JAMES, L. A. FRANKS, et al. CZT device with improved sensitivity for medical imaging and homeland security applications. In: *Hard X-Ray, Gamma-Ray, and Neutron Detector Physics XI*. SPIE Proceedings Vol. 7449, 2009, 744902-744912. DOI: 10.1117/12.828514. IBSN 1996-756X.

[4] TRAVERSA, M., P. PRETE, I. FARELLA, P. PAIANO, F. MARZO, A. COLA, N. LOVERGINE and A. M. MANCINI. A MOVPE technology for fabrication of CdTe-based homoepitaxial p-i-n diode structures as nuclear radiation detectors. In: *2007 2nd International Workshop on Advances in Sensors and Interface*. IEEE, 2007, s. 1-5. DOI: 10.1109/IWASI.2007.4420028. ISBN 9781424412440.

[5] TOMASHIK, Z. F., V. M. TOMASHIK, I. B. STRATIYCHUK, G. M. OKREPKA, I. I. HNATIV, P. MORAVEC, P. HÖSCHL and J. BOK. Chemical–Mechanical Polishing of CdTe and Zn x Cd1−x Te Single Crystals by H2O2(HNO3)–HBr–Organic Solvent Etchant Compositions. *Journal of Electronic Materials*. 2009,**38**(8), 1637-1644. DOI: 10.1007/s11664-009-0692-8. ISSN 03615235.

[6] NILES, D. W., X. LI, P. SHELDON and H. HÖCHST. A photoemission determination of the band diagram of the Te/CdTe interface. *Journal of Applied Physics*. 1995, **77**(9), 4489 - 4495. DOI: 10.1063/1.359444.. ISSN 1089-7550.

[7] GORICHOK, I. V., P. M. FOCHUK, Y. V. VERZHAK, T. O. PARASHCHUK, D. M. FREIK, O. E. PANCHUK, A. E. BOLOTNIKOV and R. B. JAMES. Compensation mechanism of bromine dopants in cadmium telluride single crystals. *Journal of Crystal Growth*. 2015, **415**, 146-. DOI: 10.1016/j.jcrysgro.2014.11.005. ISSN 00220248.

[8] KELLER, R. C., H. ZIMMERMANN, M. SEELMANN-EGGEBERT and H. J. RICHTER. Surface cleaning and etching of CdZnTe and CdTe in H2/Ar, CH4/H2/Ar, and CH4/H2/N2/Ar electron cyclotron resonance plasmas.*Journal of Electronic Materials*. 1997, **26**(6), 542-. DOI: 10.1007/s11664-997-0191-8. ISSN 03615235.

[9] MAINZER, N., E. LAKIN a E. ZOLOTOYABKO. Point-defect influence on 1/f noise in HgCdTe photodiodes. *Applied Physics Letters*. 2002, **81**(4), 763-766. DOI: 10.1063/1.1494118. ISSN 00036951.

[10] VAN DER ZIEL, A. Unified presentation of 1/f noise in electron devices: fundamental 1/f noise sources.*Proceedings of the IEEE*. **76**(3), 233-258 [cit. 2016-08-29]. DOI: 10.1109/5.4401. ISSN 00189219.

[11] CHOO, S.C. Carrier generation-recombination in the space-charge region of an asymmetrical p-n junction. *Solid-State Electronics*. 1968, **11**(11), 1069-1077. DOI: 10.1016/0038-1101(68)90129-9. ISSN 00381101.

[12] SHOCKLEY, W. and W. T. READ. Statistics of the Recombinations of Holes and Electrons. *Physical Review*. 1952, **87**(5), 835-842. DOI: 10.1103/PhysRev.87.835. ISSN 0031-899x

[13] BALANDIN, A. A. *Noise and fluctuations control in electronic devices*. 1. Stevenson Ranch, Calif.: American Scientific Publishers, 2002. ISBN 1588830055.

[14] COLA, A. and I. FARELLA. The polarization mechanism in CdTe Schottky detectors. *Applied Physics Letters*. 2009, **94**(10), 102113-102117. DOI: 10.1063/1.3099051. ISSN 00036951.

[15] HOOGE, F. N. 1/f noise sources. *IEEE Transactions on Electron Devices*. 1994, **41**(11), 1926-1935. DOI: 10.1109/16.333808. ISSN 00189383.

[16] CHATTOPADHYAY, K., X. MA, J. O. NDAP, et al. Thermal treatments of CdTe and CdZnTe detectors. In:*Hard X-Ray, Gamma-Ray, and Neutron Detector Physics II*. Dan Diego, USA: Proc. SPIE 4141, 2000. DOI: 10.1117/12.407595. ISSN 1996-756X.

[17] HERRMANN, W. A. (ed.). *Synthetic methods of organometallic and inorganic chemistry (Herrmann/Brauer)*. Stuttgart: Georg Thieme Verlag, 2000. ISBN 0865779716.

[18] SIMON, A. Group 1 and 2 suboxides and subnitrides — Metals with atomic size holes and tunnels.*Coordination Chemistry Reviews*. 1997, **163**, 253-270. DOI: 10.1016/S0010-8545(97)00013-1. ISSN 00108545

[19] EVERSON, W. J., C. K. ARD, J. L. SEPICH, B. E. DEAN, G. T. NEUGEBAUER and H. F. SCHAAKE. Etch pit characterization of CdTe and CdZnTe substrates for use in mercury cadmium telluride epitaxy. *Journal of Electronic Materials*. 1995, **24**(5), 505-510. DOI: 10.1007/BF02657954. ISSN 03615235

[20] SZELES, C., S. E. CAMERON, J. O. NDAP and W. C. CHALMERS. Advances in the crystal growth of semi-insulating CdZnTe for radiation detector applications. *IEEE Transactions on Nuclear Science*. 2002, **49**(5), 2535-2540. DOI: 10.1109/TNS.2002.803882. ISSN 00189499.

[21] SZELES, Csaba, R. B. JAMES, R. C. SCHIRATO, E. E. EISSLER, D. J. REESE and S. E. CAMERON. Radiation detector performance of CdTe single crystals grown by the conventional vertical Bridgman technique. In:*Hard X-Ray, Gamma-Ray, and Neutron Detector Physics*. San Diego: Proc. SPIE 3768, 1999, s. 98-106. DOI: 10.1117/12.366626. ISSN 1996-756X.

[22] REESE, M. O., C. L. PERKINS, J. M. BURST, et al. Intrinsic surface passivation of CdTe. *Journal of Applied Physics*. 2015, **118**(15), 155305. DOI: 10.1063/1.4933186. ISSN 00218979.

[23] ROUSE, A. A., C. SZELES, J. O. NDAP, et al. Interfacial chemistry and the performance of bromine-etched CdZnTe radiation detector devices. In: *2001 IEEE Nuclear Science Symposium Conference Record*. IEEE, 2002, s. 2459-2463. DOI: 10.1109/NSSMIC.2001.1009316. ISBN 0780373243.

List of selected publications – published in journals with Impact factor

A1. ŠIK, O., P. BÁBOR, P. ŠKARVADA, M. POTOČEK, T. TRČKA, L. GRMELA and E. BELAS. Investigation of the effect of argon ion beam on CdZnTe single crystals surface structural properties. *Surface and Coatings Technology: ACCEPTED, IN PRINT* . DOI: 10.1016/j.surfcoat.2016.05.006. ISSN 02578972.

A2. ŠIK, O., L. GRMELA, H. ELHADIDY, et al. Study of electric field distribution and low frequency noise of CdZnTe radiation detectors. *Journal of Instrumentation*. IOP, 2013, **8**(C06005), 1-5. DOI: 10.1088/1748-0221. ISSN 17480221.

A3. ŠIK, O., ŠKARVADA, GRMELA, O. ŠIK, P. ŠKARVADA, L. GRMELA, J. ŠIKULA and J. FRANC. Contact quality analysis and noise sources determination of CdZnTe-based high-energy photon detectors. *Physica Scripta*. IOP, 2013,**T157**(2013), 1-4. DOI: 10.1088/0031-8949/2013/T157/014064. ISSN 1402-4896.

A4. ELHADIDY, H., R. GRILL, J. FRANC, O. ŠIK, P. MORAVEC and O. SCHNEEWEISS. Ion electromigration in CdTe Schottky metal–semiconductor–metal structure. *Solid State Ionics*. 2015, **278**, 20-25. DOI: 10.1016/j.ssi.2015.04.016. ISSN 01672738.

A5. ANDREEV, A., O. SIK, L. GRMELA and J. SIKULA. Ageing of Cadmium Telluride Radiation Detectors and its Diagnostics with Low Frequency Noise. *Metrology and Measurement Systems*. 2013-01-1, **20**(3), 385–394. DOI: 10.2478/mms-2013-0033. ISSN 08608229.

A6. KNÁPEK, A., L. GRMELA, J. ŠIKULA and O. ŠIK. Cold Field-Emission Cathode Noise Analysis. *Metrology and Measurement Systems*. 2012-01-1, **19**(2), 417-422. DOI: 10.2478/v10178-012-0036-5. ISSN 0860-8229

Curriculum Vitae

Profesional experience

2012 - 2016 — PhD student
Central European Institute of Technology
Analysis of transport and noise properties of CdTe- based IR/ gamma ray semiconductor detectors

2006 – 2009 — SMT technician
DuHa system, Brno
Operation of pick-and-place SMT system

Prototypes testing, firmware programming, PCB design

Education

1999 – 2003 — **Secondary Technical School Zlin,** electrical engineering and radio communications

2003 – 2008 — **Brno university of Technology**, MsC degree in programme "Electrical, Electronic, Communication and Control Technology".

2008 – 2016 — PhD, **Brno university of Technology**, branch Physical Electronics and nanotechnology. PhD thesis " Study of Transport, Noise and Structural Properties of CdTe Radiation Detectors".

Fellowships abroad

2014 — 2 months at Faculty of Engineering and Physical Sciences at the University of Surrey, UK. α particle Time-of-Flight measurements.

2015 — 2 months at National Research Council of Italy, Lecce division. Current Transient Technique and Pockels effect measurements.

Profesional skills

Skilled in pulsed (Time-of-Flight, Current Transient Technique) methods of semiconductor electrical quantities - charge carrier mobility, lifetime, trapping, direct mapping of electric field distribution by the Pockels Effect, Current voltage and noise characteristics analysis. Currently, I am interested in surface analysis by XPS, Auger Spectroscopy, Low Energy Ion scattering and in vibrathonic methods like FTIR, Raman spectroscopy, Cathodoluminiscence.

Computer and Language Skills

Czech, English (proficient, CEFR C1), Spanish (low) and Russian (low).Word, Excel, Matlab, Origin – advanced user

Hobbies and interests:

Sports, mainly swimming and cycling, gardening; discovering cultures around the world, literature; physics and new technologies.

Participated Projects:

GA15-05259S, Surface passivation of CdTe/CdZnTe radiation detectors, started 01.01.2015.

GAP102/11/0995, Electron transport, Noise and Diagnostic of Shottky and Autoemission Cathodes, 01.01.2011 - 31.12.2013

GD102/09/H074, Diagnostika defektů v materiálech za použití nejnovějších defektoskopických metod, 01.01.2009 - 31.21.2012